doi: 10.1038/nature06964

Anatase TiO_2 single crystals with a large percentage of reactive facets

Hua Gui Yang, Cheng Hua Sun, Shi Zhang Qiao, Jin Zou, Gang Liu, Sean Campbell Smith, Hui Ming Cheng & Gao Qing Lu

Part I: Calculation section

(1) Structural models. In each case, stoichiometric slab models (1×1) are employed: consisting of 9 atomic layers and a total of 9 atoms for clean (001) surface, 8 atomic layers and a total of 12 atoms for clean (101) surface. For the above (001) and (101) surfaces, each surface contains one fivefold Ti, which is terminated by X (X = H, B, C, N, O, F, Si, P, S, Cl, Br, I). All atoms are relaxed without any constraint.

(2) Computational methods. All calculations have been carried out using the density functional theory (DFT) within the generalized-gradient approximation (GGA) [1], with the exchange-correlation functional of Perdew-Burke-Ernzerhof (PBE) [2, 3]. This has been implemented in the Vienna ab initio simulation package (VASP) [4,5], which spans reciprocal space with a plane-wave basis, in this case up to a kinetic energy cutoff of 450 eV. The pseudopotential configurations that yielded the minimum energies for all involved structures included: the {3p4s3d} electrons for Ti (Ti_sv), $\{1s^2\}$ for H, $\{2s^22p^1\}$ for B, $\{2s^22p^2\}$ for C, $\{2s^22p^3\}$ for N, $\{2s^22p^4\}$ for O, $\{2s^22p^5\}$ for F, $\{3s^23p^2\}$ for Si, $\{2s^22p^3\}$ for P, $\{3s^23p^4\}$ for S, $\{3s^23p^5\}$ for Cl, $\{4s^24p^5\}$ for Br, $\{5s^25p^5\}$ for I. We have used an 11×11×11 Monkhorst-Pack k-point mesh for bulk anatase, 11×11×1 for slabs, 3×3×3 for dimers of X for the final calculations of energies. During the relaxations all structures have been relaxed to an

energy convergence of 10^{-4} eV (equating to a force convergence of 10^{-2} eV/Å). In the case of slabs, the vacuum space is larger than 15 Å. And for the dimers of X, a cubic unit cell with a = b = c = 16 Å has been employed. For isolated atoms (to correct the cohesive energy), a unit cell with a = 15 Å, b = 16 Å, c = 17 Å has been used.

(3) Reliability of methods and results. To check the reliability of the above methods, several tests have been performed.

(i) Cohesive energy per TiO_2 of bulk anatase is -21.60 eV, which is very close to Lazzeri's result (-21.54 eV by PBE [6]);

(ii) Cohesive energy of H_2 is 435.99 kJ/mol, which is highly consistent with the experimental result (436.0 kJ/mol [7]);

(iii) Surface energies of clean (001) and (101) surfaces are 0.93 J/m^2 and 0.39 J/m^2 respectively, which is close to Lazzeri's result (0.90 J/m^2 and 0.44 J/m^2 [6]). We also got values of 0.96 J/m^2 and 0.41 J/m^2 using the exchange-correlation functional of Perdew and Wang (PW91).

Calculations of surface free energy (**γ**)

Based on previous studies [8-14], **γ** is calculated by,

$$\gamma = \frac{E^{slab} - NE_{TiO2}^{bulk} - N_X E_X}{2A} \qquad (1)$$

where, E_{TiO2}^{bulk} is the energy per unit of TiO_2, E^{slab} is the total energy of the slab, N is the total number of unit TiO_2 contained in the slab model, N_X is the number of adsorbed X atoms, $E_X = \frac{1}{2}E_{X-X}$, and $E_{X\text{-}X}$ indicates the total energy of dimer X_2.

(4) Details for extensive tests based on (4×4) slab models

To exclude the possible errors due to the small size of (1×1) slabs, (4×4) supercell is also employed for the calculation of the surface free energies of (001), which can be helpful to clarify the stabilization effect of fluorine atoms.

a) Calculation details

exchange-correlation functional: GGA/PBE [2]

pseudopotential for core electrons: Effective core potential [15]

basis set: Double-numeric quality basis set [16,17]

b) Tests

Test 1:

Bonding energy for bulk anatase TiO_2

1×1 unit cell: -21.5441 eV; 4×4 supercell: -21.0410 eV

Test 2:

1×1 model: $\gamma_{001} = 0.94$ J/m^2 $\gamma_{F\text{-}001} = -0.61$ J/m^2

($\gamma_{001} = 0.92$ J/m^2 by VASP) ($\gamma_{F\text{-}001} = -0.55$ J/m^2 by VASP)

c) Calculated results:

4×4 model: $\gamma_{001} = 0.97$ J/m^2 $\gamma_{F\text{-}001} = -0.66$ J/m^2

From the above calculated results, it is clear that the (4×4) and (1×1) slab models give the same conclusion that the coverage of F can stabilize the surfaces dramatically.

(5) Discussion of the stabilization mechanism of fluorine atoms supported by first principle calculations

To understand the stabilization effect resulted by fluorine atoms, first principle calculations are employed. Based on the optimized structures, geometries and electronic structures are discussed thoroughly.

a) Analysis of displacements normal to the surfaces

The relaxed clean and fluorated surfaces are shown in Fig. S1 (a)-(d), with Ti, O and F being labeled as gray, red and cyan spheres respectively. Moreover, fivefold-Ti, sixfold-Ti, twofold-O (bridging oxygen) and threefold-O are indicated as Ti1, Ti2, O1, and O2, respectively. Atomic displacements normal to the surfaces in the uppermost

layer have been listed in Table S1 for clean and fluorated surfaces. Comparisons have been drawn with results of Lazzeri et al. [6]) and Barnard et al. [14] for clean surfaces. In the case of clean surfaces, it can be summarized that: (i) both O1 and O2 tend to relax toward the vacuum, resulting in a remarkable distortion of the T-shaped bonding structure formed by O2 and its three neighbouring titaniums; and (ii) in the case of Ti, only Ti1 tends to move outward. According to Burdett et al. [18], the bulk structure of anatase is controlled by the balance between the O-O repulsions (which mainly determine the Ti-O bond length) and the attractive Ti-O π interactions (which mainly determine the planarity of the T-shaped bonding structure). Lazzeri et al. confirmed this view and further pointed out that the O-O repulsions appear to be the most important factor [6]. Due to the cleavage of surfaces, such balance has been broken and oxygen atoms on the surface tend to move outward since no O-O repulsion prevents such relaxation. In the case of fluorated surfaces, two important changing tendencies can be proposed: (i) oxygen atoms except O2 on F-(001) move inward remarkably; and (ii) Ti1 is the outmost. Both (i) and (ii) are related to the strong electronegativity of the fluorine atoms, which introduce strong F-O repulsion and Ti-F attraction (bonding energies of Ti-F is as high as 569.0 kJ/mol [19]). Thereby, a new balance between O-O/F-O repulsions and Ti-O/Ti-F attractions can be constructed, which stabilize Ti and O atoms on the surfaces.

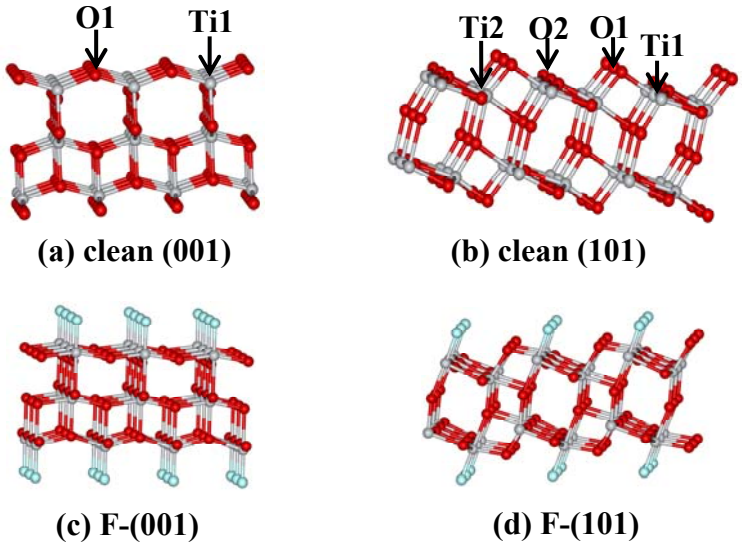

Figure S1 Relaxed clean and fluorated surfaces of anatase. (**a**) clean (001); (**b**) clean (101); (**c**) F-(001); (**d**) F-(101). Ti, O and F are labelled as gray, red and cyan spheres respectively.

Table S1 Displacements (in Å), normal to the surface, of atoms in the uppermost layer. Positive and negative displacement indicates outward and inward movements.

Surface	Label	Coordination	Ref. 14	Ref. 6	This work	Fluorated
(001)	O1	2	0.08	0.20	**0.37**	**-0.46**
	O2	3	-0.06	0.04	**0.04**	**0.08**
	Ti1	5	-0.02	0.05	**0.16**	**0.23**
(101)	O1	2	-0.02	0.06	**0.20**	**-0.07**
	O2	3	0.19	0.28	**0.34**	**-0.04**
	Ti1	5	-0.18	-0.12	**0.00**	**0.21**

b) Electronic structures

To further understand the stabilization mechanism related to the fluorine atoms, an investigation of electronic structures of clean and F-terminated surfaces has been carried out. As a reference, DOS of bulk anatase TiO_2 is calculated and shown in Fig. S2. Combining the projected DOS (PDOS, as shown in Fig. S2 (a)) and partial DOS

(Fig. S2 (b)), three features can be summarized: (i) in the range of -17.71 to 4.78 eV, there are three regions, lower valence band (VB) located at about -17.71 eV to -15.99 eV, upper VB at around -4.82 eV to 0.00 eV, and conduction band (CB) at around 2.00 eV to 4.78 eV; (ii) lower VB, upper VB and CB mainly consist of O_{2s}, O_{2p} and Ti_{3d} orbitals, respectively; and (iii) for O_{2s}, only one peak is observed, while CB is decomposed into Ti e_g (>5 eV) and t_{2g} (<5 eV). The band width of the upper VB is 4.82 eV, which is highly consistent with early XPS results (4.75 eV) [20], and comparable to Asahi's result (5.05 eV from FPLAPW [21]).

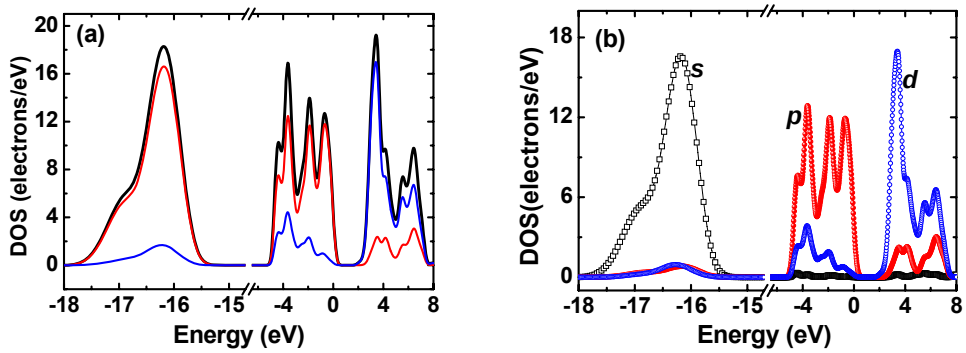

Figure S2 Calculated DOS for bulk anatase TiO_2. (**a**) Total (black) and projected DOS contributed by O (red) and Ti (blue); (**b**) Partial DOS contributed by various orbitals.

DOS and PDOS of fluorated surfaces are shown in Fig. S3, with cyan, red and blue lines for F, O and Ti respectively. To investigate the surface effect, the contributions of O1 and O2 are further separated and drawn in the sets of Fig. S3 (a)-(d). In the case of clean surfaces (Fig. S3 (a)-(b)), two interesting features are observed with respect to the perfect crystal shown in Fig. S2: (i) electrons contributed by Ti_{3d} delocalize in the whole range of the higher VB; and (ii) the lower VB (mainly O_{2s}) is decomposed into two peaks and the gaps between the O_{2s} peaks of O1 and O2 are 1.0 eV and 1.8 eV for clean (001) and (101) respectively. With the formation of Ti-F, however,

localized states of Ti_{3d} are observed, and the gaps between the O_{2s} peaks of O1 and O2 decrease remarkably, as shown in Fig. S3 (c)-(d), suggesting that fluorine atoms stabilize not only titanium atoms but also unsaturated oxygen atoms, which is consistent with the shortening of the bond length of Ti1-O1 as discussed above. In fact, both Ti_{3d} and O_{2p} can interact with F_{2p} according to the DOS and PDOS shown in Fig. S3 (c)-(d) and thus Ti-F (attractive) and O-F (repulsive) interactions can be expected, which stabilize unsaturated Ti and O atoms on the surfaces.

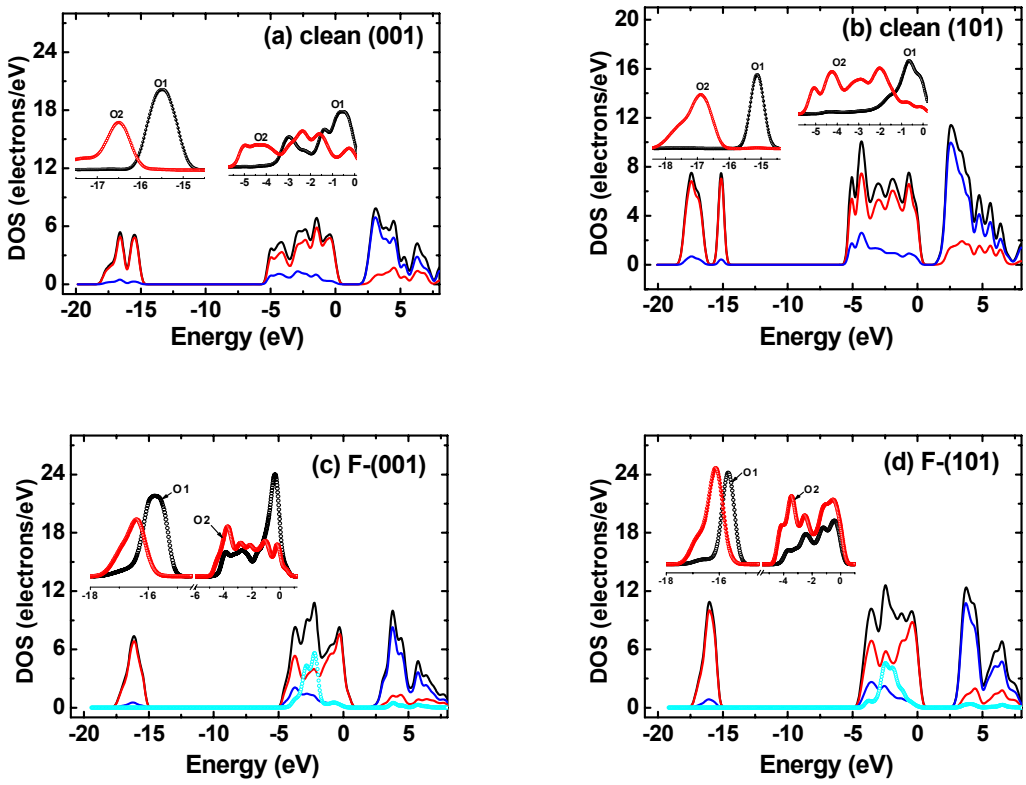

Figure S3 Total (black) and projected density of states (PDOS, with cyan, red and blue lines for F, O and Ti) calculated for surfaces of anatase. (**a**) clean 001; (**b**) F-001; (**c**) clean 101; (**d**) F-101. PDOS ranging from -18.0 eV to 1.0 eV contributed by O1 and O2 are also shown in the insets with black and red symbols, respectively.

According to the above analysis of the geometries and electronic structures, a new balance between the O-O/F-O repulsions and the Ti-O/Ti-F attractions can be

constructed due to the interactions of Ti_{3d}-F_{2p} and O_{2p}-F_{2p}, which stabilize Ti and O atoms on the surfaces.

References:

[1] Kohn, W. & Sham, L. J. Self-consistent equations including exchange and correlation effects. *Phys. Rev. B* **140**, A1133 - A1138 (1965).

[2] Perdew, J. P., Burke, K. & Ernzerhof, M. Generalized gradient approximation made simple. *Phys. Rev. Lett.* **77**, 3865 - 3868 (1996).

[3] Kresse, G. & Joubert, D. From ultrasoft pseudopotentials to the projector augmented-wave method. *Phys. Rev. B* **59**, 1758 - 1775 (1999).

[4] Kresse, G. & Furthmüller, J. Efficient iterative schemes for ab initio total-energy calculations using a plane-wave basis set. *Phys. Rev. B* **54**, 11169 - 11186 (1996).

[5] Kresse, G. & Furthmüller, J. Efficiency of ab-initio total energy calculations for metals and semiconductors using a plane-wave basis set. *Comput. Mater. Sci.* **6**, 15 - 50 (1996).

[6] Lazzeri, M., Vittadini, A. & Selloni, A. Structure and energetics of stoichiometric TiO_2 anatase surfaces. *Phys. Rev. B* **63**, 155409 (2001).

[7] Zmbov, K. F. & Margrave, J. L. Mass spectrometric studies at high temperatures. XVI. Sublimation pressures for titanium(III)fluoride and the stabilities of TiF_2(g) and TiF(g). *J. Phys. Chem.* **71**, 2893 - 2895 (1967).

[8] Wang, X.-G. et al. The hematite (α- Fe_2O_3) (0001) surface: evidence for domains of distinct chemistry. *Phys. Rev. Lett.* **81**, 1038 -1041 (1998).

[9] Wang, X.-G., Chaka, A. & Scheffler, M. Effect of the environment on α-Al_2O_3 (0001) surface structures. *Phys. Rev. Lett.* **84**, 3650 - 3653 (2000).

[10] Reuter, K. & Scheffler, M. Composition, structure, and stability of RuO_2 (110) as a function of oxygen pressure. *Phys. Rev. B* **65**, 035406 (2002).

[11] Lo, C. S., Tanwar, K. S., Chaka, A. M. & Trainor, T. P. Density functional theory study of the clean and hydrated hematite (1102) surfaces. *Phys. Rev. B* **75**, 075425 (2007).

[12] Wang, H. Y. & Schneider, W. F. Effects of coverage on the structures, energetics, and electronics of oxygen adsorption on RuO_2 (110). *J. Chem. Phys.* **127**, 064706 (2007).

[13] Barnard, A. S., Zapol, P. & Curtiss, L. A. Anatase and rutile surfaces with adsorbates representative of acidic and basic conditions. *Surf. Sci.* **582**, 173 - 188 (2005).

[14] Barnard, A. S. & Zapol, P. Effects of particle morphology and surface hydrogenation on the phase stability of TiO_2. *Phys. Rev. B* **70**, 235403 (2004).

[15] Bergner, A., Dolg, M., Küechle, W., Stoll, H.& Preuss, H. Ab *initio* energy-adjusted pseudopotentials for elements of groups 13-17. *Mol. Phys.* **80**, 1431 – 1441 (1993).

[16] Delley, B. An all-electron numerical method for solving the local density functional for polyatomic molecules. *J. Chem. Phys.* **92**, 508 - 517 (1990).

[17] Delley, B. From molecules to solids with the $DMol^3$ approach. *J. Chem. Phys.* **113**, 7756 - 7764 (2000).

[18] Burdett, J. K., Hughbanks, T., Miller, G. J., Richardson, J. W. & Smith, J. V. Structural-electronic relationships in inorganic solids: powder neutron diffraction studies of the rutile and anatase polymorphs of titanium dioxide at 15 and 295 K. *J. Am. Chem. Soc.* **109**, 3639 - 3646 (1987).

[19] Huber, K. P. & Herzberg, G. Molecular spectra and molecular structure. IV. Constants of diatomic molecules. 642 (Van Nostrand Reinhold, New York, 1979).

[20] Sanjinés, R. et al. Electronic structure of anatase TiO_2 oxide. *J. Appl. Phys.* **75**, 2945 - 2951 (1994).

[21] Asahi, R., Taga, Y., Mannstadt, W. & Freeman, A. J. Electronic and optical properties of anatase TiO_2. *Phys. Rev. B* **61**, 7459 - 7465 (2000).

Part II: Experiment section

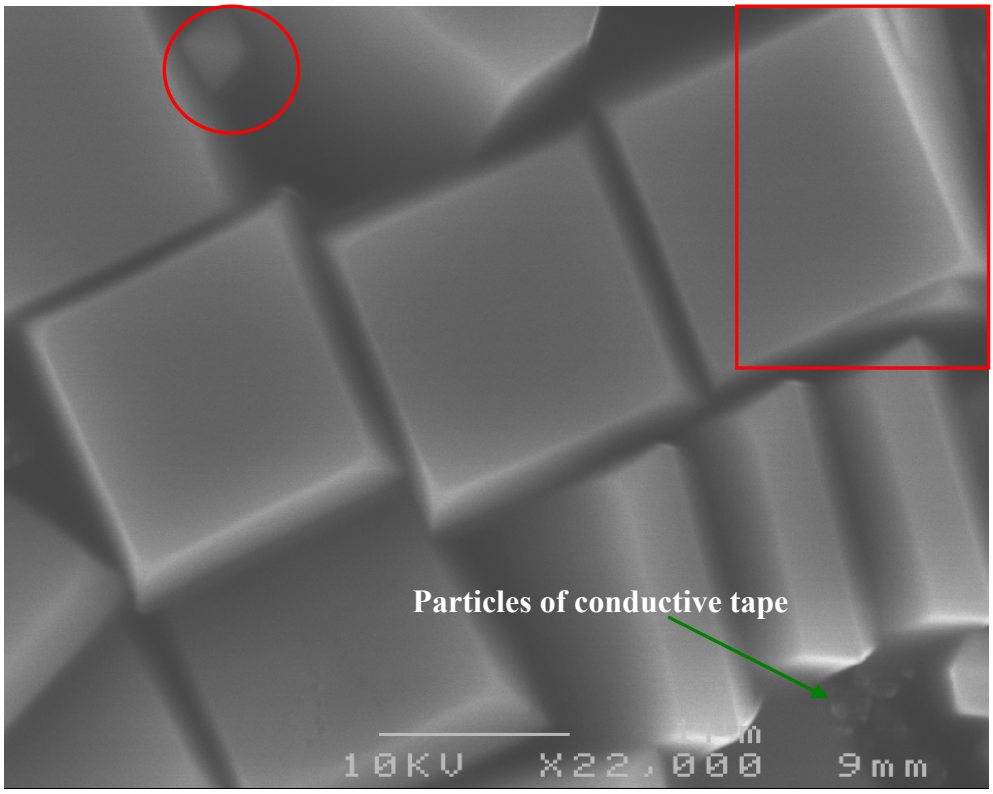

Figure S4 Some typical agglomerated anatase single crystals (indicated by red rectangle) and irregular particles (indicated by red circle) in the samples.

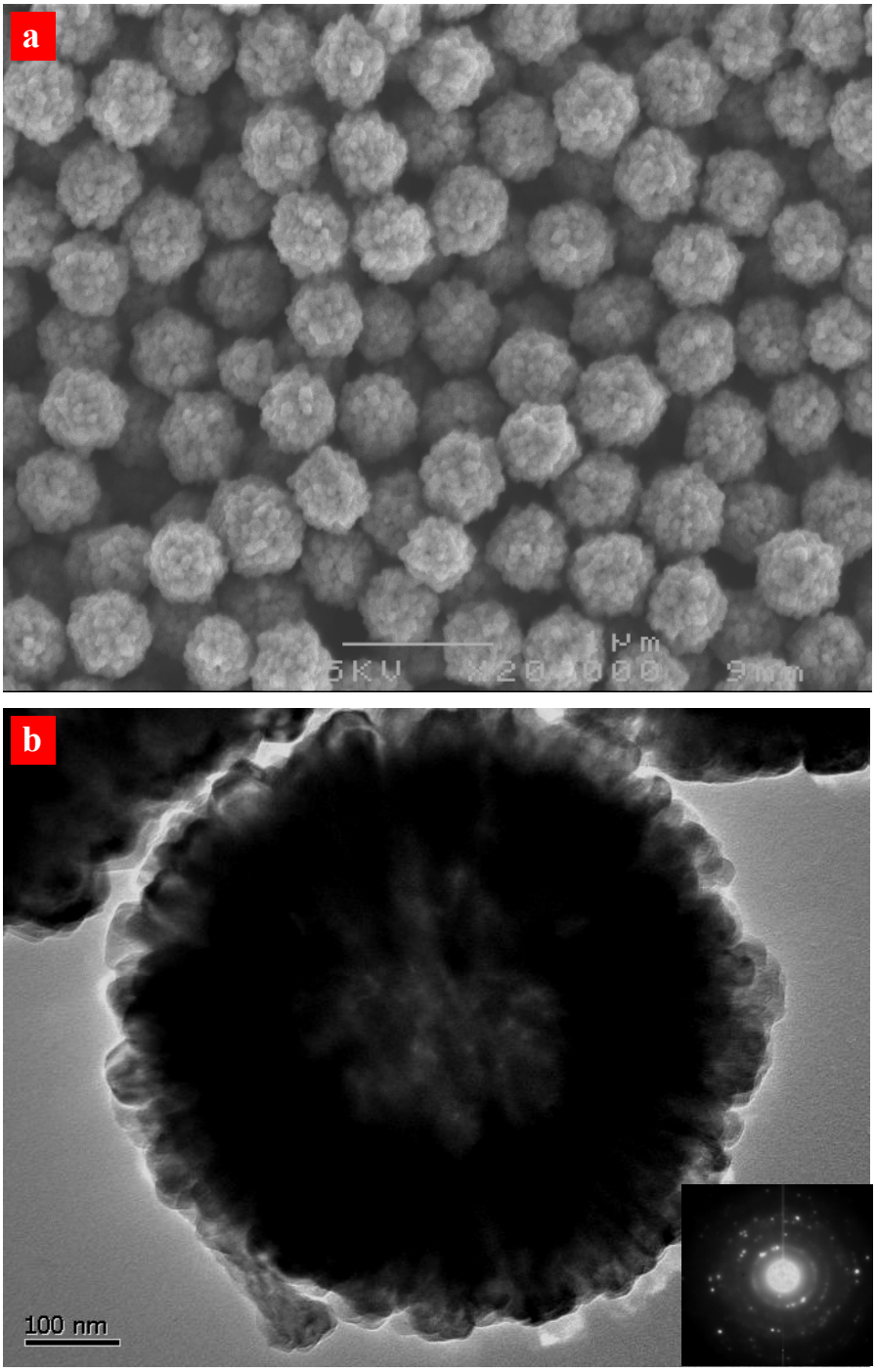

Figure S5 Control experiments for the synthesis of anatase crystals without adding additional HF. (**a**) **&** (**b**), SEM/TEM images of typical polycrystalline particles. Experimental conditions: 2.67 mM titanium tetrafluoride (TiF_4) aqueous solution, at 180 ^{o}C for 20 h. The inserted selected-area electron diffraction pattern is the evidence for the polycrystalline structure of the particles.

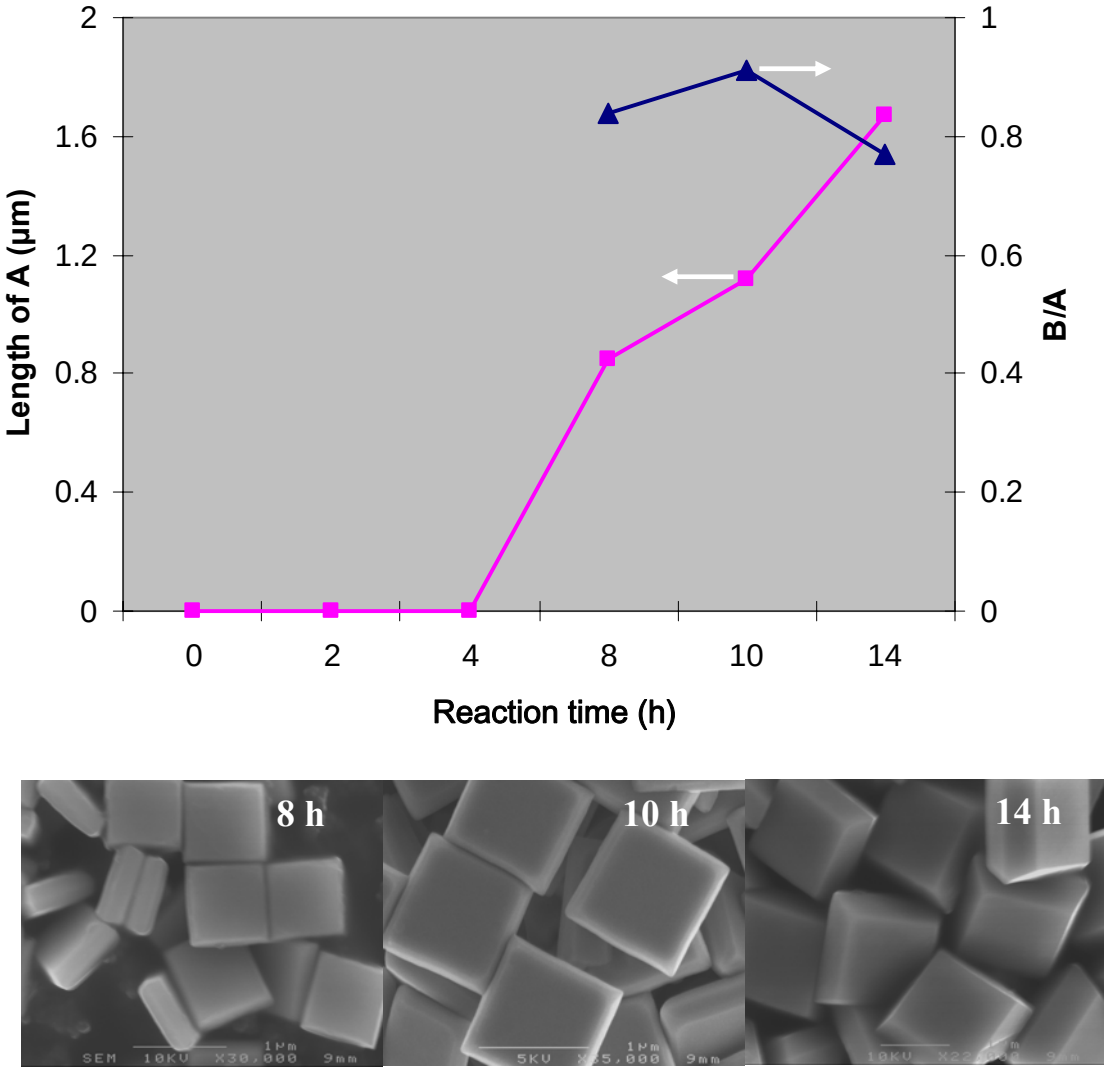

Figure S6 Anatase single crystals with a shorter reaction time show a smaller size and a higher degree of truncation. For example, anatase single crystals with A = 850 nm and B/A = 0.84 on average could be prepared with a reaction time of 8h. All the experimental parameters are the same as those presented in Figure 2a, except the reaction time.

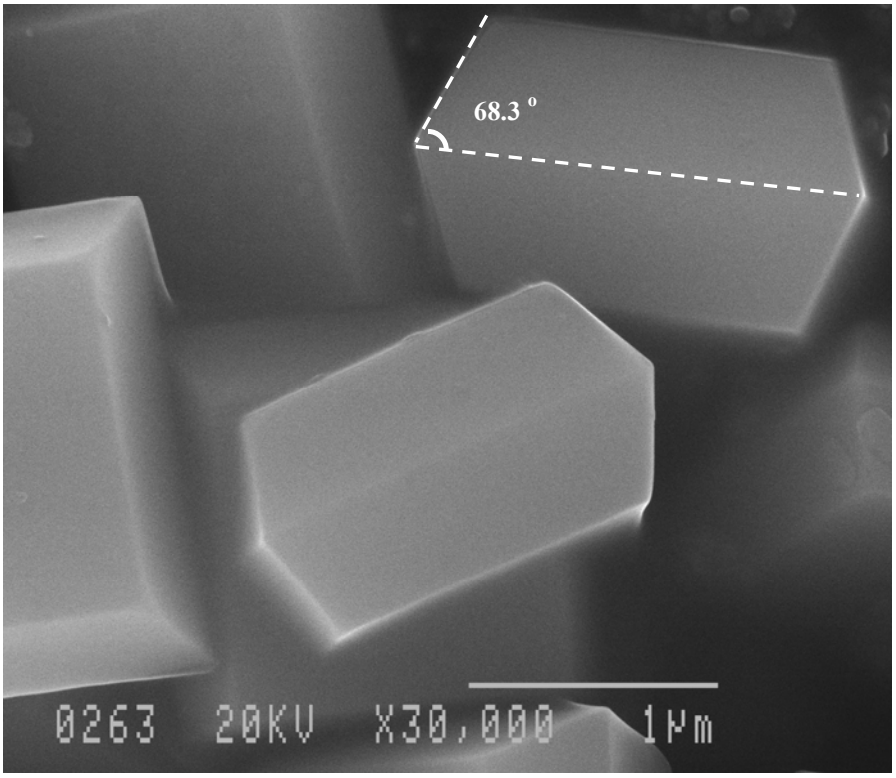

Figure S7 Interfacial angle between {001} and {101} facets (68.3 ± 0.3° on average). The white dashed lines indicate the (001) and (101) crystal planes of anatase TiO_2, respectively.

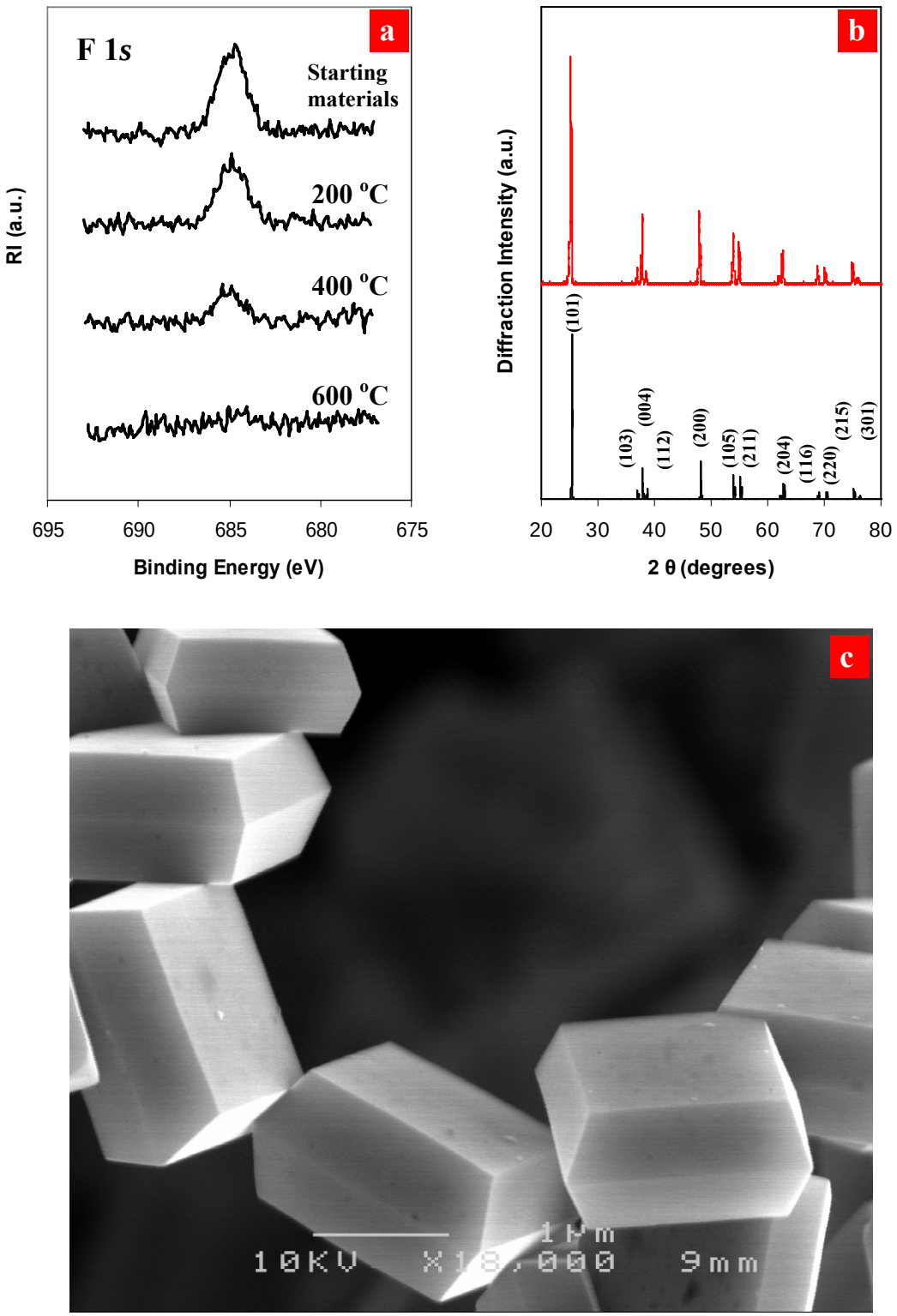

Figure S8 Defluorination study using anatase single crystals shown in Figure 2a as starting materials. (**a**), XPS spectra of initial anatase single crystals and anatase single crystals heated at 200 °C, 400 °C, and 600 °C for 90 min. (**b**) **&** (**c**), XRD pattern and SEM image of anatase single crystals heated at 600 °C for 90 min. Calculated X-ray diffraction pattern of bulk anatase is also shown ((**b**), bottom). The average values of A and B/A of the heated sample are 1.74 μm and 0.79 respectively, which are all comparable with the anatase single crystals without heat treatment.